Published in final edited form as:
Radiat Res. 2013 January ; 179(1): 9–20. doi:10.1667/RR3089.1.

Chromosome Damage in Human Cells by γ Rays, α Particles and Heavy Ions: Track Interactions in Basic Dose-Response Relationships

Bradford D. Loucas[a,1], **Marco Durante**[b], **Susan M. Bailey**[c], and **Michael N. Cornforth**[a]

[a]Department of Radiation Oncology, The University of Texas Medical Branch, Galveston, Texas

[b]Biophysics Department, GSI Helmholtzzentrum für Schwerionenforschung, Darmstadt, Germany

[c]Department of Environmental and Radiological Health Sciences, Colorado State University, Fort Collins, Colorado

Abstract

We irradiated normal human lymphocytes and fibroblasts with ^{137}Cs γ rays, 3.5 MeV α particles and 1 GeV/amu ^{56}Fe ions and measured the subsequent formation of chromosome-type aberrations by mFISH at the first mitosis following irradiation. This was done for the purposes of characterizing the shape of dose-response relationships and determining the frequency distribution of various aberration types with respect to the parameters of dose, radiation quality and cell type. Salient results and conclusions include the following. For low-LET γ rays, lymphocytes showed a more robust dose response for overall damage and a higher degree of upward curvature compared to fibroblasts. For both sources of high-LET radiation, and for both cell types, the response for simple and complex exchanges was linear with dose. Independent of all three parameters considered, the most likely damage outcome was the formation of a simple exchange event involving two breaks. However, in terms of the *breakpoints* making up exchange events, the majority of damage registered following HZE particle irradiation was due to complex aberrations involving multiple chromosomes. This adds a decidedly nonlinear component to the overall breakpoint response, giving it a significant degree of positive curvature, which we interpret as being due to interaction between ionizations of the primary HZE particle track and long-range δ rays produced by other nearby tracks. While such track interaction had been previously theorized, to the best of our knowledge, it has never been demonstrated experimentally.

INTRODUCTION

Ionizing radiation (IR) comes in many forms, ranging from sparsely ionizing X and γ rays, to densely ionizing charged particles from natural alpha emitters and heavier high-energy (HZE) ions. These radiations are generally categorized by their ionization density in terms of linear energy transfer (LET), defined as the amount of energy deposited per unit track length (1). Low-LET radiations (e.g., <2 keV/μm) produce curvilinear dose responses for chromosome aberration induction (2, 3). Most of the microscopically visible damage resulting from exposure to IR takes the form of chromosomal exchange-type aberrations. As

[1]Address for correspondence: Department of Radiation Oncology, Biology Division, 1.132 Brackenridge Hall, Rt. 0884, The University of Texas Medical Branch, 301 University Blvd., Galveston, TX 77555; bdloucas@utmb.edu.

The online version of this article (DOI: 10.1667/RR3089.1) contains supplementary information that is available to all authorized users.

is commonly the case, we confine our discussion to the genesis of chromosome-type exchanges observed at the first mitosis following irradiation.

According to the tenets of the most popular models of aberration formation (4), chromosome exchanges result from the interaction of two or more breaks in close spatial and temporal proximity (i.e., they are proximate), more specifically the misrejoining of broken chromosome ends that such breaks produce. The overall yield of exchanges (Y) as a function of dose (D) is curvilinear in shape and is usually described as a second-order polynomial of the familiar form $Y = \alpha D + \beta D^2$, where the α coefficient applies to the linear portion of the curve, and the β coefficient is responsible for any upward curvature in the dose response. The linear portion is thought to be the consequence of the misrejoining of break pairs formed by ionizations that occur along a single electron track that is set in motion by photo-absorptive events (5). These events dominate at low doses and low dose rates and are independent of dose rate. At higher doses and dose rates contribution from the β coefficient begins to dominate and the interaction of breaks caused by *independent* electron tracks becomes more likely. This process also leads to misrejoining involving two or more breaks, and results in a dose-dependent curvature in the dose response, which is profoundly affected by dose rate.

X- or γ-rays (via secondary electrons) deposit very small amounts of energy per unit track length, and so require a large number of tracks to produce a substantial dose. Moreover, the mass of electrons is extremely low causing them to be easily scattered. Taken together, these characteristics result in a more-or-less random spatial distribution of ionizations within a target volume. In stark contrast, low-energy charged particles, such as those from naturally emitted α particles have a much higher LET and produce densely spaced ionizations distributed among far fewer tracks to achieve the same dose. Otherwise the same basic concepts involving the interaction of multiple proximate breaks apply. However, since the average distance between α-particle tracks for a given dose is much greater compared to that for low-LET tracks, high-LET track interaction is effectively eliminated for any dose that is likely to be used in an experimental setting. Thus, chromosome exchange formation is effectively confined to interactions of breaks caused by single-track action. Consequently linear dose responses are observed that are independent of dose rate.

High-LET radiations also produce low-LET secondary electrons that emanate radially from the primary track. For lower energy α particles, the length of such δ rays is limited to a few nanometers, which effectively precludes their interaction with damage produced by other (independent) primary tracks (6). Energy deposition by high-LET radiations from high atomic number high-energy (HZE) particles evokes additional considerations with regard to aberration formation. This is because a significant portion of the energy delivered by such species is deposited by secondary electrons in the form of δ rays ejected from the primary track that can, in some cases, travel up to centimeter distances. Here, track interaction becomes a distinct possibility, either with fellow electrons produced by an independent primary track or, more likely, with the core of such a track itself. We postulate that such track interactions should be detectable, as curvature in the chromosome aberration dose response.

To test this hypothesis, we used 24-color mFISH (7) to assess simple and complex chromosome aberration formation following irradiation of human lymphocytes with 1 GeV/amu Fe ions. For comparison, we conducted similar analyses after irradiation of normal human fibroblasts with 3.5 MeV ^{238}Pu α particles. We discuss implications of these findings, including possible effects of dose rate that are implied by such a mechanism, and results will be compared to our previously published results for γ rays in both cell types (8, 9).

The current study is the first of a planned pair of studies that will discuss the production of chromosome aberrations by low-energy α particles compared to HZE particles in normal human cells. Here, we address basic dose-response relationships for the production of exchange-type aberrations. In articles to follow we will address, issues pertaining to the formation of "open breaks" (e.g., terminal deletions and incomplete exchanges).

MATERIALS AND METHODS

Culture Conditions and Irradiations

Lymphocytes and Fe irradiations—Venous blood from a healthy volunteer was drawn into a Vacutainer CPT (Beckton-Dickinson, Lincoln Park, IL). The Vacutainer tube was centrifuged for 30 min at 3,000 rpm, the buffy coat was carefully removed and resuspended in PBS, and was spun for 10 min at 1,500 rpm. After two further washes in PBS, the white blood cells were resuspended in RPMI-1640 medium (Gibco BRL, Grand Island, NY) supplemented with 20% fetal bovine serum. A 2 ml volume of the suspension, at a concentration of approximately 10^6 cells/ml, was loaded by syringe into specially constructed Lucite holders. Both the loading chamber and the holder wall facing the beam were 1 mm thick. Cells were exposed in air at room temperature to 1 GeV/amu ^{56}Fe ions at the NASA Space Radiation Laboratory, Brookhaven National Laboratory (Upton, NY). Beam uniformity in the irradiated area was checked using an X-ray film, and was ≤5%. The dose rate was approximately 1 Gy/min. Physical characteristics and dosimetry of the 1 GeV/amu ^{56}Fe beam were described in detail by Zeitlin *et al.* (10). The dose- and track-average LET in water of this beam are 147 keV/μm and 142 keV/μm, respectively. If we assume that each human lymphocyte is a sphere with a radius of approximately 3 μm, then a dose of 83 cGy roughly corresponds to an average of one Fe-ion track traversal per cell nucleus. Immediately after exposure, lymphocytes were aspirated from the holder using a syringe and were transferred into a T25 tissue culture flask containing 10 ml of RPMI-1640 medium supplemented with 1% phytohaemagglutinin (PHA; Gibco). Cultures were allowed to grow for 46 h before Colcemid (0.2 μg/ml final concentration) was added 2 h prior to the harvest of mitotic cells. In addition, Calyculin (50 m*M* final concentration) was added to Colcemid-blocked cultures 45 min before harvest to induce premature chromosome condensation (PCC) in G_2 phase cells (11). Consequently, chromosome spreads resulting from this treatment represented a mixture of G_2 PCC and mitotic chromosomes. Harvested cells were fixed in 3:1 methanol to acetic acid by standard cytogenetic procedures and transported to the University of Texas Medical Branch at Galveston for analysis.

Fibroblasts and α-particle irradiations—α-Particle irradiation experiments were conducted at the Los Alamos National Laboratory using low passage AG1521 normal primary human fibroblasts and following procedures described previously (12). Briefly, low passage cells originally obtained from the NIA cell repository (Coriell Institute, Camden, NJ) were revived from frozen stocks into Dulbecco's modified Eagle's medium (DMEM) supplemented with 10% fetal bovine serum, penicillin and streptomycin. These were maintained at 37°C in a humidified atmosphere of 95% air/5% CO_2. Four days prior to irradiation, 1×10^5 cells were plated onto 1.5 μm thick Mylar surfaces forming the bottom of 28 mm diameter dishes. On the day of the experiment, confluent monolayers of cells were irradiated through the Mylar membranes with graded doses of ^{238}Pu α particles at a dose rate of 3.48 cGy/s (13). Under the conditions used here, the incident energy of the particles was calculated to be 3.5 MeV. This corresponds to an LET of 116 keV/μm, which was estimated to remain essentially unchanged as the particles passed through the cell. Immediately after irradiation the cells were returned to the incubator where they remained for 24 h. After incubation, cells were trypsinized and subcultured into T-75 tissue culture flasks and returned to the incubator. Colcemid was added to one flask at each dose 28 h

post-subculture and to a second flask 4 h later. Mitotic cells were harvested after a 4 h Colcemid treatment and fixed in 3:1 methanol and acetic acid, as above. Mitotic indices were determined and the collection period yielding the highest index for each data point was used in further analyses. Data from γ-ray experiments used for comparisons were published previously (8, 9) and details of the procedures used can be found there.

mFISH analysis—Hybridization and karyotyping were conducted as described previously (8). Briefly, fixed cells were spread onto glass microscope slides and treated with acetone, RNase A and proteinase K before fixation in 3.7% formaldehyde. Slides were dehydrated through an ethanol series (70, 85 and 100%) and air dried before incubation in 72°C formamide (70%) in 2×SSC (0.3 *M* NaCl, 0.03 *M* sodium citrate) for 2 min to denature the chromosomal DNA. After dehydration through another ethanol series, 10 μl of denatured (10 min at 72°C) SpectraVision 24-color mFISH Assay probe (Vysis) was applied to each slide. Slides were covered with a 22 × 22 mm glass cover slip sealed into position with rubber cement. Samples were allowed to hybridize for 48 h in a 37°C incubator. After hybridization, cover slips were removed and the slides were washed for 2 min in 0.4× SSC containing IGEPAL (0.3%) nonionic detergent at 72°C. This was followed by a 30 s wash in 2×SSC (0.1% IGEPAL) at room temperature. Finally, 15 μl of DAPI (0.144 μg/ml) dissolved in VectaShield anti-fade mounting medium (Vector Laboratories) was applied to each slide and covered with a 24 × 40 mm cover slip.

Images of chromosome spreads were captured using a Zeiss Axiophot epifluorescence microscope equipped with a SensSys black and white CCD camera. Karyotypes were constructed from as many chromosome spreads as possible on each slide using PowerGene image analysis software. Metaphase cells were analyzed by following procedures that were previously established (8). First, mPAINT descriptors were assigned to chromosomes involved in aberrations (14). Next, each rearrangement was brought to “pattern closure” by grouping elements in the most conservative way possible, minimizing the number of exchange breakpoints required. Reciprocal pairwise rejoinings between one (as in the case of ring formation) or two chromosomes were scored as simple exchanges. Exchanges involving three or more breakpoints were regarded as complex. This classification was also applied to incomplete exchanges where one or more elements failed to rejoin, as well as to so called “one-way” exchanges where one or more translocated segments of chromosome appeared to be missing, presumably because they were too small to be resolved by mFISH (15).

RESULTS

Complete karyotypes were constructed from each cell scored and each chromosome aberration was categorized as either a simple exchange, complex exchange or a non-exchange event (Table 1). Non-exchange aberrations, which include terminal deletions, truncated chromosomes and linear acentric fragments, are shown in column 4 of Table 1 for the purpose of expressing overall damage (see Overall Chromosome Damage section). (A detailed analysis of these lesions will be deferred to a future paper where they can be dealt with at a level of detail that is beyond the scope of this paper.)

Overall Chromosome Damage

Simple exchanges arise from the pairwise interaction (rejoining) between two breaks, either within one chromosome—as in the case of interstitial deletions or pericentric and paracentric rings—or between two chromosomes, namely dicentrics or reciprocal translocations. In contrast, complex exchanges involve a minimum of three breaks and two chromosomes for their formation, although rearrangements involving several breakpoints

and chromosomes are not uncommon (8, 16, 17). For this reason, it is often preferable to express total damage in terms of the number of breakpoints rather than as the number of exchanges themselves.

The dose responses for breakpoints from all sources following various radiation treatments are shown in Fig. 1. As is clear from the figure, α-particle irradiation of fibroblasts produced the most damage per unit dose. As would be predicted from classical theoretical considerations, the data were adequately fitted by a simple linear model. Compared to α particles, there were fewer breakpoints produced in lymphocytes by iron ions. Interestingly, and central to the major conclusions of these studies, is the fact that the dose response for these HZE particles showed a modest upward curvature that statistically justified the addition of a βD^2 term in fitting the data (F test; $P < 0.01$).

As expected, γ rays delivered to either lymphocytes or fibroblasts produced the least amount of damage per unit dose. While the data represent a relatively large number of mFISH karyotypes scored (Table 1), they are confined to only a few dose points. This probably accounts for the fact that while a curvilinear dose response is expected for such low-LET radiations, and while a degree of upward curvature seems obvious from the figure, it was not possible to justify, on statistical grounds alone, the addition of a βD^2 term ($P \geq 0.05$). Nevertheless, the curve fits shown in Fig. 1 include this term for γ rays. Fitted parameters for all radiations used in these studies are shown in Table 2. Of final note is the observation that in comparing previously published γ ray data, differential radiosensitivity was observed for lymphocytes (8) versus fibroblasts (9).

Simple Versus Complex Exchanges

To avoid potential confusion in terminology, the adjective “complex” as it is used in this study, refers to interactions among three or more chromosome breaks (i.e., DNA double-strand breaks; DSBs) that involve large (submicron) dimensions. This contrasts sharply with the meaning of the same term as used in molecular parlance to describe complex biochemical lesions in DNA associated with clustered damage, the dimensions of which are nanometer in scale, and the potential influence of which on LET-dependent damage processing has been the topic of much discussion (18–20).

In this section, we limit our discussion to damage associated with exchange-type aberrations. Here we make a distinction between the number of exchange events themselves (hereafter referred to as exchanges) and the number breakpoints required for their formation. For example, the frequency of *breakpoints* associated with simple exchanges will be exactly twofold greater than the frequency of simple exchanges from which they derive, since each such exchange is composed of two chromosome breaks. Conversely, the yield of *complex breakpoints* will be dependent on the “size” of the exchange (i.e., the number of breakpoints involved) as well as on their relative frequency within the sample population.

The data and resultant curve fits are shown in Fig. 2 where the upper row of panels refers to *exchanges*, and the lower row of panels refers to the minimum number of *breakpoints* required to produce them. By convention, fits were made for γ ray data using a linear-quadratic model that included a constant term representing the intercept although, as previously mentioned, such fits did not always justify the addition of a curvilinear (βD^2) term on statistical criteria alone. For high-LET irradiations the data were well fitted by a simple linear model, the sole exception being complex breakpoints following ^{56}Fe irradiation (2F). Details of the model used and fit parameters appear in Table 3. As shown in Table 3, a pure quadratic model was used in fitting data associated with complex rearrangements following γ irradiation, since linear-quadratic fits produced negative α coefficients.

Encapsulating the data shown in Figs. 1 and 2, and Table 1, the following observations become apparent. First, irrespective of whether one considers exchange events or their resultant breakpoints, the majority of damage produced by the three radiations examined was of the simple type. Second, the sole exception to this observation was for complex breakpoints produced by ^{56}Fe ions, whose yield dominated the response for doses above ~1 Gy. Finally, for γ ray—where a matched comparison was possible between both cell types for the same radiation—substantially greater response to damage was observed in lymphocytes compared to plateau phase fibroblasts (particularly in the case of complex exchanges).

Distribution of Damage among Cells

A distinct advantage of cytogenetic end points lies in their ability to assess biological responses on a cell-by-cell basis. This allows an assessment of chromosome damage and its distribution among cells for an irradiated population. There exists a seemingly endless number of ways that information from this large data set may be presented. Three of these are discussed below, each of which was chosen for the purpose of illustrating a particular point.

One way to display such data is to plot separate histograms of size-frequency distributions for each dose, cell and radiation type, where "size" refers to the overall number of breakpoints including both exchange- and non-exchange rearrangements. To display all of the data in this way would require 19 individual plots. From this complete data set, six representative plots were chosen for display in Fig. 3, selected on the basis of *iso-effective* doses that produced about three total breakpoints per cell. With the possible exception of the 2.0 Gy dose that was used for lymphocytes exposed to γ rays, this allowed for a good match to the data shown in Fig. 1. Whereas the mean number of chromosome breakpoints per cell increased steadily with dose, the modal number of the distributions shown in Fig. 3 remained at two. This was the case for virtually all of the 19 treatments considered, and was particularly evident for lymphocytes irradiated with 1.5 Gy of Fe ions (see Supplementary material, Fig. 1S: http://dx.doi.org/10.1667/RR3089.1.S1). Although the mean number of breakpoints rose to an extraordinary 5.2 per cell, and the distribution became decidedly skewed, the modal number did not shift from two.

Figure 4 represents a second way to display distributional data, and gives an additional sense as to what is occurring. Here, we constructed three-dimensional plots comparing the frequency of cells containing specific numbers of chromosome aberrations with the total number of breakpoints in each cell for selected treatments. Figure 4A–D represent treatment conditions that match Fig. 3A–D. As can be seen, at low γ-ray doses, most of the cells that were damaged contained a single simple exchange (n.b., on the graphs, a cell containing a simple exchange will register as one aberration, two breakpoints; likewise, a cell containing two simple exchanges will be recorded at two aberrations, 4 breakpoints and so forth). It is uniformly the case that as the dose increased, more cells were observed to contain a higher frequency of aberrations, and that these became progressively larger in size.

Panels E and F from Fig. 4 represent the highest doses given for lymphocytes exposed to either γ rays or ^{56}Fe ions, respectively. They characterize frequency distributions that are roughly iso-effective for mean total breakpoints (Fig. 1). In comparing the two panels, though, it is evident that this similarity in means belies significant differences in the way in which total breakpoints are distributed. In particular, the distribution of breaks produced by ^{56}Fe ions is more diffuse (spread out) and favors the inclusion of cells harboring a large number of breakpoints. The complete data set representing all 38 plots from which Figs. 3 and 4 derive are available in supplementary data (see supplementary materials, Fig. 1S:

http://dx.doi.org/10.1667/RR3089.1.S1; Figs. 2S: http://dx.doi.org/10.1667/RR3089.1.S2; and Fig. 3S: http://dx.doi.org/10.1667/RR3089.1.S3).

The third and final way that we have chosen to represent distributional data is illustrated in Fig. 5, where information is not displayed on a cell-by-cell basis. Instead, aberration "size" in terms of breakpoints is plotted against frequency, irrespective of the number of exchanges found in any particular cell. For example, data from a single cell having a terminal deletion, a simple exchange and a complex exchange involving five breakpoints would be binned along the x-axis as follows: one event having a single break, one event having two breaks, and one event having five breaks. As mentioned earlier, the individual panels A–D correspond to those of Figs. 3 and 4 in terms of cell type and radiation, except that in this case data for all of the doses delivered are shown.

The distributions found after irradiating either cell type with γ rays (Fig. 5A and B) exhibit modal frequencies of roughly 0.8 at 2 breakpoints, the principal difference between them being the presence of low frequencies of large complex exchanges composed of more than six breakpoints in the lymphocytes. For the α-particle irradiated fibroblasts the modal frequency fell to approximately 0.7 (Fig. 5C). Here, an increased incidence of three breakpoint exchanges was found and the largest exchange observed required eight breakpoints. Additionally, more dramatic changes were produced by Fe ions, where the modal frequency fell further to about 0.5 (Fig. 5D). This decline occurred in connection with a growing number of complex exchanges with high numbers of breakpoints, the largest involving an enormous 20 breakpoints. Clearly, the most striking feature of these four plots is their similarity in basic shape which independent of dose, showed modal frequencies all solidly centered on two.

DISCUSSION

The studies described in this paper represent a compilation of work carried out at different institutions over the span of years. As a practical matter, this did not always allow for ideal pairwise distinctions to be made across cell lines and radiations. That being said, there are a number of observations that warrant discussion, which we have elected to structure in the form of specific comparisons shown graphically in Fig. 6, and which correspond to the following four subsections.

Low- Versus High-LET Radiations

Among fibroblasts—The dose responses for total breakpoints shown in Fig. 1 exemplify clastogenic responses expected for these two broad classes of IR. For fibroblasts, this comparison involves ^{137}Cs γ rays and ^{238}Pu α particles, archetypical examples of low- and high-LET radiations, respectively. As expected on the basis of classical theory, the former shows upward curvature in the dose response, while the latter leads to a steeper response with linear dose dependency. Figure 2, panels A, B, D and E illustrate these tendencies for simple and complex exchanges in fibroblasts, for both total breakpoints and the exchanges from which they derive. For fibroblasts exposed to γ rays, complex aberrations (Fig. 2A) and their breakpoints (Fig. 2D) contribute, though somewhat modestly, to the overall shape of the dose response. In sharp contrast, complex exchanges make a significant contribution to the yield of exchanges (Fig. 2B), and an even greater contribution to breakpoints following exposure to α particles (Fig. 2E). Panels A and C from Figs. 3 and 4 illustrate the distribution of breakpoints for the iso-effective doses listed. Compared to γ rays, it is clear that α-particle irradiation leads to a shift in the profile that favors cells with a larger number of breakpoints.

Among lymphocytes—For lymphocytes the available comparison for low- versus high-LET exposures involves ^{137}Cs γ rays and 1 GeV ^{56}Fe ions, respectively. Qualitatively similar results to those mentioned above were observed for this pair of radiations, with some notable exceptions. Primary among these is the upward curvature seen in the dose response for total breakpoints following ^{56}Fe heavy ions, which differs from the characteristic linear dose response associated with α particles of similar LET. We offer the following explanation for this difference, as it represents a major conclusion of this work.

Ionizations along the trajectory of α-particle tracks are confined radially within a few nanometers. The situation for energetic heavy ions is more complicated in this regard, since they are associated with δ rays that emanate long distances from the primary track (21). We imagine that damage produced by these electrons is capable of interacting with that produced by independent particles (either the primary particles themselves or their associated δ rays) far removed from the original particle track. In theory (22), such interactions should produce the curvature in the dose response observed in Fig. 1 for total breakpoints.

It is crucial to note that exchanges themselves (both simple and complex) showed a linear dose dependency (Fig. 2C). It is only when breakpoints are considered that such curvature is evident. Furthermore, it is clear from Fig. 2F that it is solely the contribution of complex exchanges that is responsible for curvature shown in Fig. 1. This leads us to conclude that δ-ray/primary track interactions do not produce additional exchanges *per se*. Instead, they serve to "add damage" to exchanges forming along primary particle tracks, thereby allowing for the emergence of exchanges involving a growing number of breakpoints.

A final point worth mentioning is that IR-induced mitotic division delays are LET dependent (23–26). Particularly in the case of lymphocytes, this can lead to under sampling of heavily damaged cells if they do not arrive at mitosis during the Colcemid collection interval. We endeavored to lessen the potential impact of this phenomenon for Fe ion-irradiated lymphocytes through the use of Calyculin (Materials and Methods), a compound that induces premature chromatin condensation (PCC) in cycling cells, thereby allowing simultaneous assessment of damage in both G_2 and metaphase cells (11).

Intra-cell Comparisons

In this section, we confine our discussion to comparisons between fibroblasts and lymphocytes. As before, the following subsections relate to those enumerated in Fig. 6.

Low-LET among cell types—In this subsection, we compare fibroblasts with lymphocytes that are both irradiated with ^{137}Cs γ rays. From Fig. 1 it is apparent that lymphocytes display a more robust dose response for total breaks. From Table 2 it can be concluded that this difference derives principally from the fact that they display much stronger upward curvature (βD^2 term) compared to fibroblasts, as the respective α/β ratios of 1.4 and 5.0 Gy confirm. We are unaware of any previously published work that directly addresses this issue, although there are studies from which a similar conclusion can be reasonably surmised (27, 28).

High-LET among cell types—There is a dramatic increase in overall damage for fibroblasts exposed to 3.5 MeV α particles when compared to lymphocytes irradiated with 1 GeV/amu ^{56}Fe ions. Broken down further, the lighter ions produced nearly four times the number of simple exchanges and almost twice the number of complex exchanges as their HZE counterpart. Figure 6 implies the possibility of a direct comparison involving these two ion species. However, we approach any such comparison with a measure of caution because of incongruities that arise when attempting to compare two different cell types receiving two

different radiations, even for radiations that, in this case, have roughly similar LETs. In our view, the most important complicating issue in a head-to-head comparison of this type is nuclear geometry in relationship to track structure which, for any high-LET radiation delivered at experimental doses, will involve a relatively small number of tracks.

Fibroblast nuclei used in this study approximate a flattened ellipse in shape with an average thickness of 1.2 μm (29), while lymphocyte nuclei are spherical with a diameter of 5.8 μm (30). These have respective cross sectional areas of 130 μm^2 (31) and 26 μm^2. By our calculations, a fibroblast nucleus that is traversed by a single track from a 116 keV/μm α particle will receive 0.14 Gy, whereas a 147 keV/μm Fe ion crossing the nucleus of a lymphocyte will impart an average dose of 0.90 Gy. It follows that for any given dose, seven α particles will traverse a fibroblast nucleus for every one Fe ion crossing the nucleus of a lymphocyte.

The point being made here is multiple nuclear tracks are “normal” for the doses of α particles used in these studies. Hence, there is ample opportunity for inter-track action, should it occur, to express itself in the form of upward curvature in the dose response. Needless to say, such curvature was not observed; nor has there been, to our knowledge, any reports to the contrary for aberrations after exposure to α particles. On the other hand, significant curvature was observed in the overall dose response for 1 GeV iron ions across a range of doses associated with far lower fluences.

We take this as evidence in support of the following statement: Dose-response curvature (or the lack thereof) is a fundamental property of the high-LET track in question, and is not the result of complications brought about by intra-cell comparisons. This makes the presently untested prediction that curvature should also exist in the dose response for fibroblasts exposed to heavy ions. Obviously, further experiments involving direct comparisons of HZE and lighter ions are needed that use the same cell types to confirm this conclusion.

Breakpoint Distributions

The modal number of breakpoints in all four distributions shown in Fig. 5 centers on two, indicating that irrespective of dose, radiation quality, and cell type, the most likely exchange event is a simple exchange. This is in agreement with the conclusions reached by Durante *et al.* (32), but is in seeming contrast to that of Anderson and colleagues (33) who concluded that the most likely outcome following a single α-particle traversal though the nucleus of a lymphocyte was a complex exchange. The relative frequency of this modal value changes little among the panels shown, with the exception of Fig. 5D, which deals with HZE exposures. Here, the modal frequency drops noticeably to about 0.5, concomitant with an increased spread in the distribution that favors the production of complex exchanges with large numbers of breakpoints. A closer look at the extended “tail” of this distribution reveals clear evidence of dose dependency, in that all exchanges having more than 10 breaks were produced by the highest dose given. We argue that this behavior, in addition to the previously discussed curvature in the shape of the dose response, is indicative of damage interaction between two or more charged particles, specifically, the interaction of a charged particle track with the δ ray component from another track or tracks.

Concluding Remarks

An overarching consensus regarding the collective data of Figs. 3, 4 and 5 is that the most likely outcome of exposure was the production of a single simple exchange, and that all doses of Fe ions used in these studies produced heavily damaged cells whose breakpoint distribution differed substantively from the other types of radiation examined.

As regards the increased potency of α-particles compared to heavy ions in terms of overall damage, we conclude that it derives principally from the fact that the former produces ionizations that are densely concentrated within a few nanometers of the primary track. Whereas, owing to the coincident δ rays they produce, a large proportion of ionizations from HZE particles are radially dispersed long distances from the primary track's trajectory. This makes for a track for which the ionization density is essentially diluted in terms of its ability to produce the proximate breaks required for exchange type aberrations. The effect of such a track structure on the production of terminal deletions and incomplete exchanges is an altogether different matter that we will address in a subsequent article.

Because chromosome damage has long been viewed as a surrogate end point for radiogenic cancer, it has obvious implications related to health risk. NASA, in particular, has understandable interest in heavy ions from this standpoint. Much was made of the observation that ^{56}Fe ion-induced breakpoints showed statistically significant upward curvature with dose. If our explanation for this phenomenon is correct, it implies a dose-rate effect not only for X and γ rays (34, 35), but for HZE ions as well, a possibility that previously has not been given much attention. Admittedly, the fluences of HZE particles from galactic cosmic radiation (GCR) likely to be encountered in deep space are orders of magnitude lower than those associated with the range of doses we have used here (36), and it is doubtful that dose-rate effects for such radiations would apply directly to manned space travel. However, it also should be recognized that ground-based experiments designed to mimic GCR necessarily involve much higher doses (and dose rates) that require extensive extrapolation into relevant dose ranges. Such extrapolation, we argue, should be guided by biophysical principles that we are seeking to establish.

Supplementary Material

Refer to Web version on PubMed Central for supplementary material.

Acknowledgments

The authors wish to thank Drs. Edwin Goodwin and Dudley Goodhead for insightful discussions. This research was supported by Department of Energy grant number DE-FG03-02ER63442 and NASA/OBPR. Additional funding was provided by NASA (NNJ04HD83G and NNX08AB65G) and NIH/NIAID (R01080486-02).

References

1. Zirkle, RE. The radiobiological importance of linear energy transfer. In: Hollaender, A., editor. Radiation biology. New York: McGraw-Hill; 1954. p. 315-50.
2. Lea DE, Catcheside DG. The mechanism of the induction by radiation of chromosome aberrations in *Tradescantia*. J Genet. 1942; 44:216–45.
3. Lea, DE. Actions of radiations on living cells. Cambridge: Cambridge University Press; 1955.
4. Savage JRK. A brief survey of aberration origin theories. Mutat Res. 1998; 404:134–47.
5. Kellerer AM, Rossi HH. The theory of dual radiation action. Curr Top Radiat Res Q. 1972; 8:85–158.
6. Cucinotta FA, Nikjoo H, Goodhead DT. Model for radial dependence of frequency distributions for energy imparted in nanometer volumes from HZE particles. Radiat Res. 2000; 153:459–68. [PubMed: 10761008]
7. Speicher MR, Ballard SG, Ward DC. Karyotyping human chromosomes by combinatorial multi-fluor FISH. Nat Genet. 1996; 12:368–75. [PubMed: 8630489]
8. Loucas BD, Cornforth MN. Complex chromosome exchanges induced by gamma rays in human lymphocytes: An mFISH study. Radiat Res. 2001; 155:660–71. [PubMed: 11302762]

9. Loucas BD, Eberle R, Bailey SM, Cornforth MN. Influence of dose rate on the induction of simple and complex chromosome exchanges by gamma rays. Radiat Res. 2004; 162:339–49. [PubMed: 15447049]
10. Zeitlin C, Heilbronn L, Miller J. Detailed characterization of the 1087 MeV/nucleon iron-56 beam used for radiobiology at the alternating gradient synchrotron. Radiat Res. 1998; 149:560–9. [PubMed: 9611094]
11. Durante M, Furusawa Y, Majima H, Kawata T, Gotoh E. Association between G2-phase block and repair of radiation-induced chromosome fragments in human lymphocytes. Radiat Res. 1999; 151:670–6. [PubMed: 10360786]
12. Cornforth MN, Goodwin EH. The dose-dependent fragmentation of chromatin in human fibroblasts by 3. 5-MeV alpha particles from ^{238}Pu: Experimental and theoretical considerations pertaining to single-track effects. Radiat Res. 1991; 127:64–74. [PubMed: 2068273]
13. Inkret WC, Eisen Y, Harvey WF, Koehler AM, Raju MR. Radiobiology of alpha-particles: 1. Exposure system and dosimetry. Radiat Res. 1990; 123:304–10. [PubMed: 2217728]
14. Cornforth MN. Analyzing radiation-induced complex chromosome rearrangements by combinatorial painting. Radiat Res. 2001; 155:643–59. [PubMed: 11302761]
15. Wu H, George K, Yang TC. Estimate of true incomplete exchanges using flourescence *in situ* hybridization with telomere probes. Int J Radiat Biol. 1998; 73:521–7. [PubMed: 9652809]
16. Simpson PJ, Savage JR. Estimating the true frequency of x-ray-induced complex chromosome exchanges using fluorescence in situ hybridization. Int J Radiat Biol. 1995; 67:37–45. [PubMed: 7852815]
17. Griffin CS, Marsden SJ, Stevens DL, Simpson P, Savage JR. Frequencies of complex chromosome exchange aberrations induced by 238Pu alpha-particles and detected by fluorescence in situ hybridization using single chromosome-specific probes. Int J Radiat Biol. 1995; 67:431–9. [PubMed: 7738406]
18. Ward JF. Some biochemical consequences of the spatial distribution of ionizing radiation-produced free radicals. Radiat Res. 1981; 86:185–95. [PubMed: 7015409]
19. Jenner TJ, deLara CM, O'Neill P, Stevens DL. Induction and rejoining of DNA double-strand breaks in V79 mammalian cells following gamma- and alpha-irradiation. Int J Radiat Biol. 1993; 64:265–73. [PubMed: 8105005]
20. Hada M, Georgakilas AG. Formation of clustered DNA damage after high-LET irradiation: A review. J Radiat Res. 2008; 49:203–10. [PubMed: 18413977]
21. Katz R, Cucinotta FA, Zhang CX. The calculation of radial dose from heavy ions: Predictions of biological action cross sections. Nucl Instrum Methods Phys Res Sect B-Beam Interact Mater Atoms. 1996; 107:287–91.
22. Chatterjee A, Schaefer HJ. Microdosimetric structure of heavy ion tracks in tissue. Radiat Environ Biophys. 1976; 13:215–27. [PubMed: 981514]
23. Ritter S, Nasonova E, Scholz M, KraftWeyrather W, Kraft G. Comparison of chromosomal damage induced by x-rays and Ar ions with an LET of 1840 keV/amu in G(1) V79 cells. Int J Radiat Biol. 1996; 69:155–66. [PubMed: 8609451]
24. Testard I, Dutrillaux B, Sabatier L. Chromosomal aberrations induced in human lymphocytes by high-LET irradiation. Int J Radiat Biol. 1997; 72:423–33. [PubMed: 9343107]
25. George K, Wu H, Willingham V, Furusawa Y, Kawata T, Cucinotta FA. High- and low-LET induced chromosome damage in human lymphocytes: A time-course of aberrations in metaphase and interphase. Int J Radiat Biol. 2001; 77:175–83. [PubMed: 11236924]
26. Lee R, Nasonova E, Hartel C, Durante M, Ritter S. Chromosome aberration measurements in mitotic and G(2)-PCC lymphocytes at the standard sampling time of 48 h underestimate the effectiveness of high-LET particles. Radiat Environ Biophys. 2011; 50:371–81. [PubMed: 21479955]
27. Ostashevsky JY. Higher-order structure of interphase chromosomes and radiation-induced chromosomal exchange aberrations. Int J Radiat Biol. 2000; 76:1179–87. [PubMed: 10993629]
28. Wu H, Durante M, George K, Yang TC. Induction of chromosome aberrations in human cells by charged particles. Radiat Res. 1997; 148:S102–7. [PubMed: 9355863]

29. Cornforth MN, Schillaci ME, Goodhead DT, Carpenter SG, Wilder ME, Sebring RJ, et al. Radiobiology of ultrasoft x-rays: II. Normal human-fibroblasts and the significance of terminal track structure in cell inactivation. Radiat Res. 1989; 119:511–22. [PubMed: 2772142]

30. Anderson RM, Marsden SJ, Wright EG, Kadhim MA, Goodhead DT, Griffin CS. Complex chromosome aberrations in peripheral blood lymphocytes as a potential biomarker of exposure to high-LET alpha-particles. Int J Radiat Biol. 2000; 76:31–42. [PubMed: 10665955]

31. Loucas BD, Geard CR. Initial damage in human interphase chromosomes from alpha particles with linear energy transfers relevant to radon exposures. Radiat Res. 1994; 139:9–14. [PubMed: 8016313]

32. Durante M, George K, Wu H, Cucinotta FA. Karyotypes of human lymphocytes exposed to high-energy iron ions. Radiat Res. 2002; 158:581–90. [PubMed: 12385635]

33. Anderson RM, Stevens DL, Goodhead DT. M-fish analysis shows that complex chromosome aberrations induced by alpha-particle tracks are cumulative products of localized rearrangements. Proc Natl Acad Sci U S A. 2002; 99:12167–72. [PubMed: 12205292]

34. Cornforth MN. Perspectives on the formation of radiation-induced exchange aberrations. DNA Repair. 2006; 5:1182–91. [PubMed: 16807139]

35. Cornforth, MN.; Bedford, JS. Ionizing radiation damage and its early development in chromosomes. In: Lett, JT.; Sinclair, WK., editors. Advances in radiation biology. San Diego: Academic Press; 1993. p. 423-96.

36. Cucinotta FA, Durante M. Cancer risk from exposure to galactic cosmic rays: Implications for space exploration by human beings. Lancet Oncol. 2006; 7:431–5. [PubMed: 16648048]

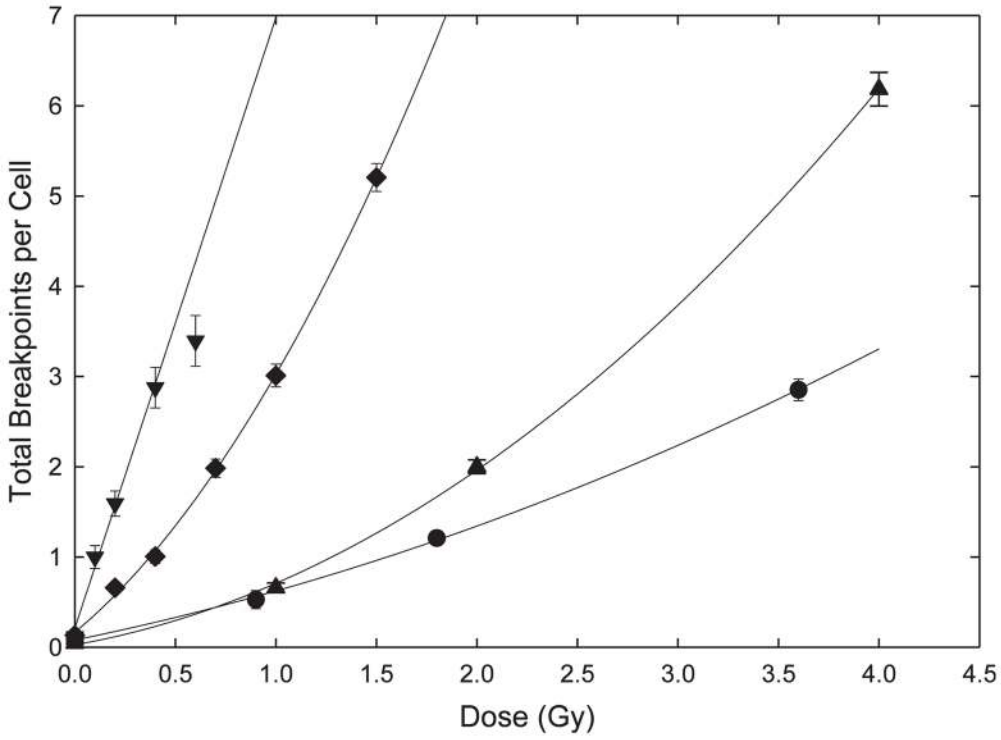

FIG. 1.

Total chromosome breakpoints per cell. The minimum number of chromosome breaks required to produce each aberration is determined from the number of color junctions or open breaks that are required to produce the mFISH pattern observed. These are totaled and expressed here as the mean number of breakpoints per cell. The error bars represent standard deviations assuming a Poisson distribution. Lines represent least squared fits to the data (see Table 2 for parameters). (●) γ-irradiated fibroblasts, (▲) γ-irradiated lymphocytes, (◆) ^{56}Fe ion-irradiated lymphocytes and (▼) α-particle irradiated fibroblasts.

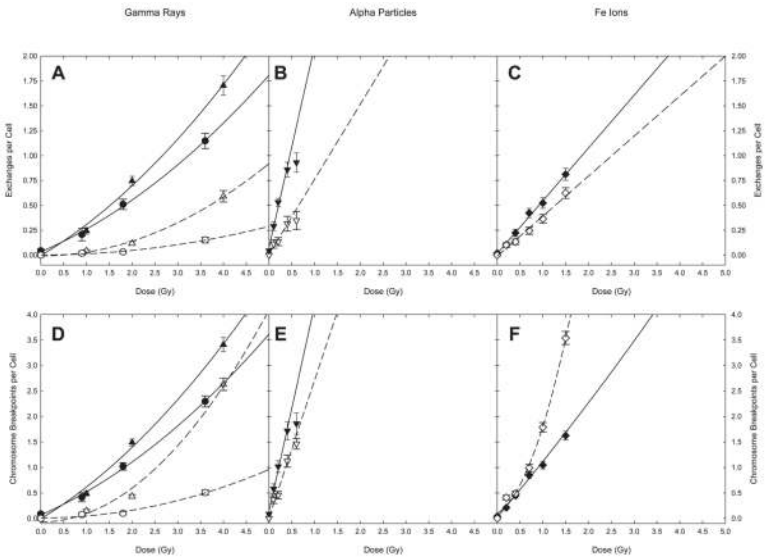

FIG. 2.

Simple and complex exchanges. Panels A–C: exchanges per cell. Panels D–E: breakpoints per cell. The error bars represent standard deviations assuming a Poisson distribution. Lines represent least squared fits to the data (see Table 3 for parameters). Solid symbols and lines: simple exchanges; open symbols and dashed lines: complex exchanges. (●, ○) γ-irradiated fibroblasts; (▲, △) γ-irradiated lymphocytes; (◆,◇) ^{56}Fe ion-irradiated lymphocytes and (▼, ▽) α-particle irradiated fibroblasts.

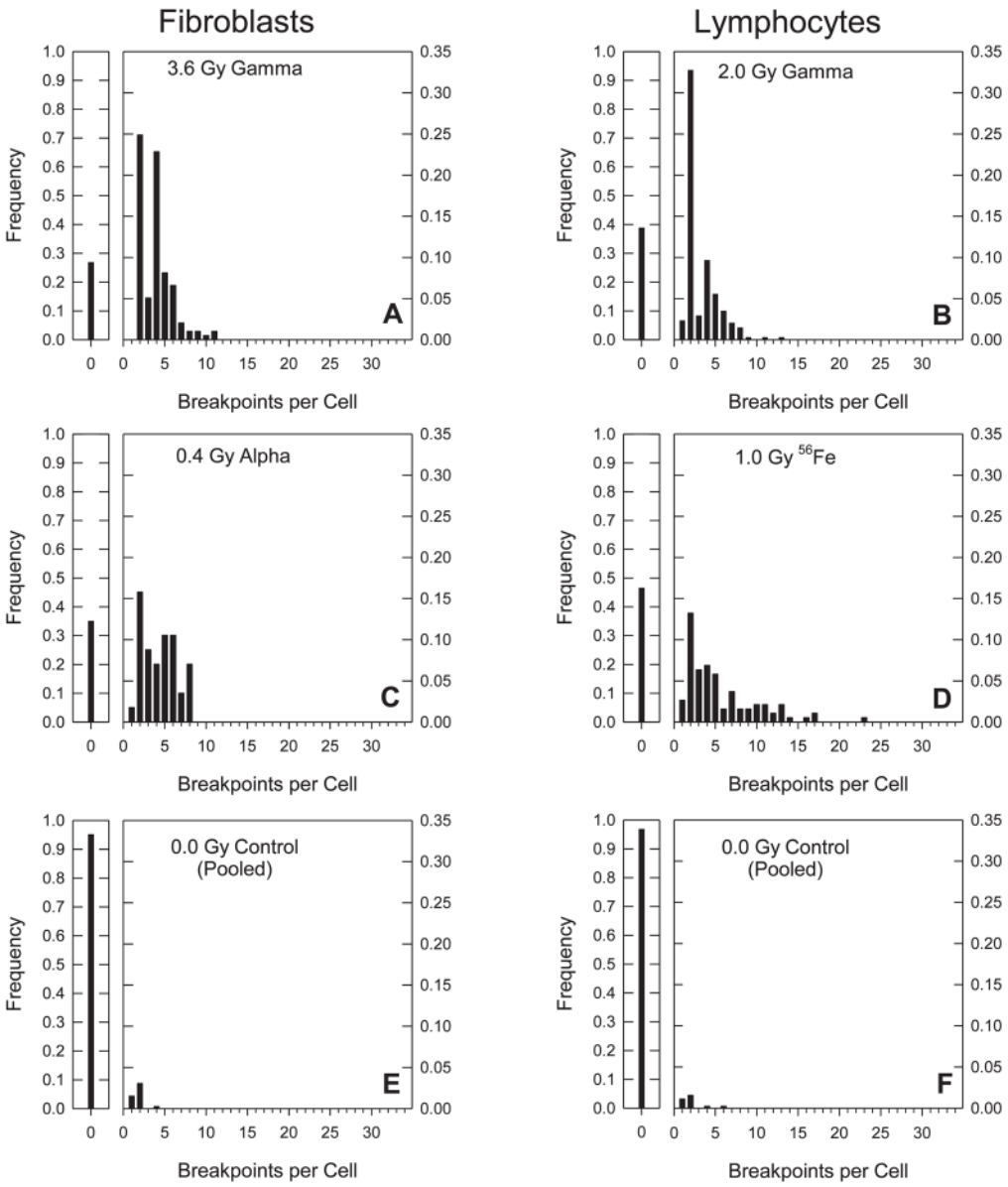

FIG. 3.

Frequency distributions of breakpoints per cell. In each panel, small graphs to the left of the main plot show the frequency of undamaged cells. Panels A–D represent breakpoint distributions for isoeffective doses (see text). Panels E and F show distributions for the unirradiated controls.

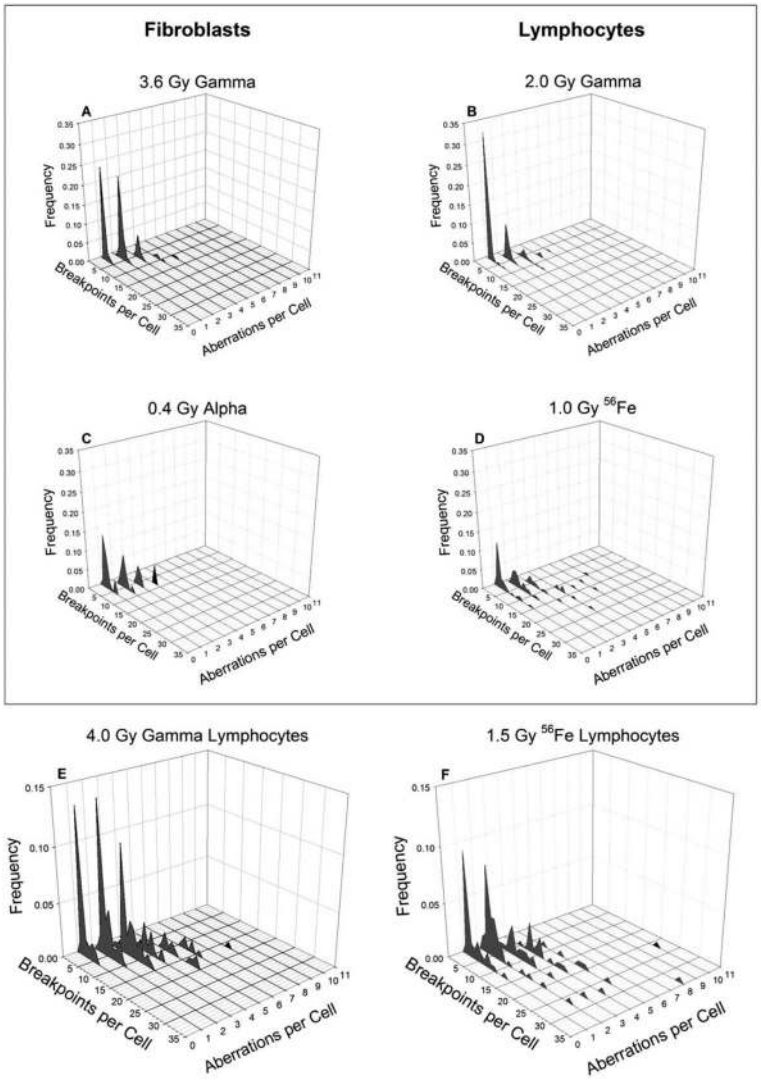

FIG. 4.

Frequency distributions of breakpoints versus chromosome aberrations per cell. This figure compares the frequency of breakpoints in cells with specific numbers of aberrations. NB: a cell with a single simple exchange (2 breakpoints) will be recorded at 2 breakpoints, 1 aberration. A cell with two simple exchanges will be recorded at 4 breakpoints, 2 aberrations and so forth. Panels A–D correspond to panels A–D on Fig. 3. Panels E and F represent the highest doses delivered to lymphocytes and do not correspond to the iso-effective doses plotted in Fig. 3. The frequency axes on these panels are also plotted on a different scale.

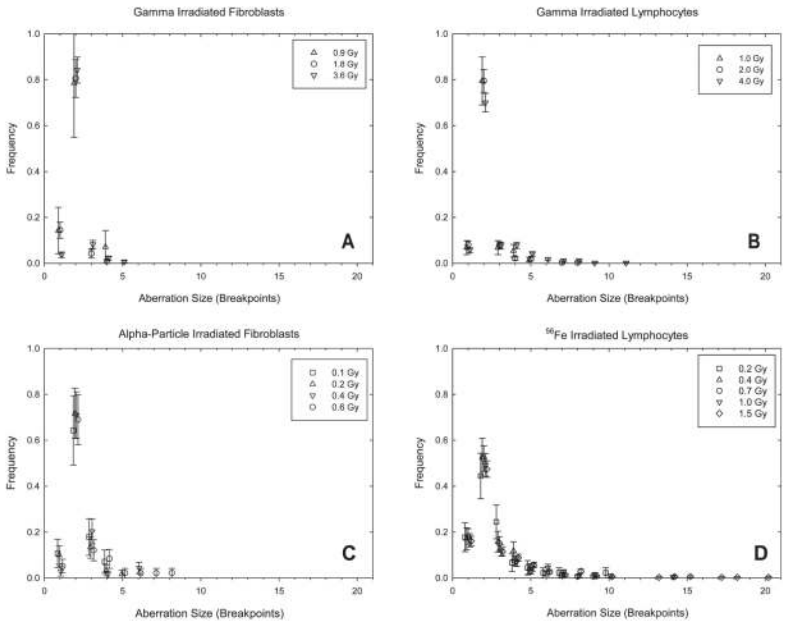

FIG. 5.

Frequency distributions of chromosome aberration size. Sizes of chromosome aberrations in terms of breakpoints are plotted as frequencies relative to the total number of aberrations. Points for each dose are offset around a specific size to allow greater clarity. The error bars represent standard deviations assuming a Poisson distribution. Panel A: γ-irradiated fibroblasts, (△) 0.9 Gy, (○) 1.8 Gy and (▽) 3.6 Gy. Panel B: γ-irradiated lymphocytes, (△) 1 Gy, (○) 2 Gy and (▽) 4 Gy. Panel C: α-irradiated fibroblasts, (□) 0.1 Gy, (△) 0.2 Gy, (▽) 0.4 Gy and (○) 0.6 Gy. Panel D: Fe ion-irradiated lymphocytes, (□) 0.2 Gy, (△) 0.4 Gy, (○) 0.7 Gy, (▽), 1.0 Gy and (◇) 1.5 Gy.

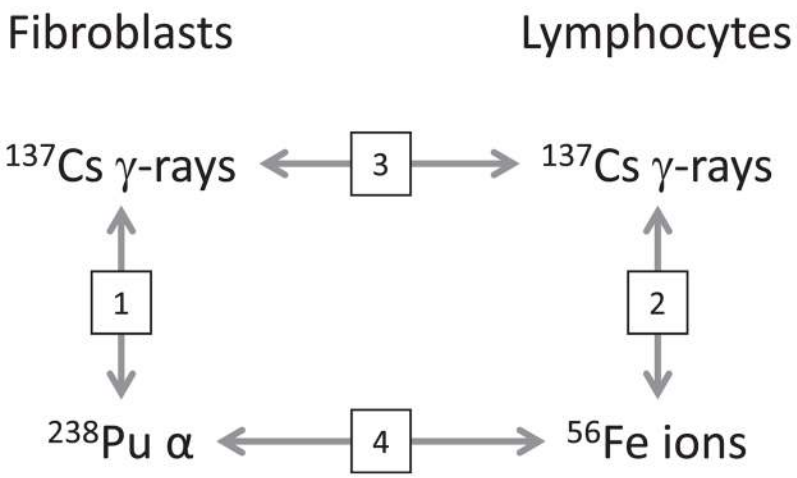

FIG. 6.

Diagram of available comparisons between fibroblasts and lymphocytes exposed to low-LET ^{137}Cs γ rays and high-LET radiations from either ^{238}Pu α particles or ^{56}Fe heavy ions. The four comparisons are numbered to correspond to the appropriate subsections of the Discussion section.

TABLE 1

Chromosome Damage

Cells radiation	Dose (Gy)	Number of cells scored	Non-exchange aberrations	Simple exchanges	Complex exchanges	Complex exchange breakpoints
Lymphocytes γ rays (8)	0	354	2	7	0	0
	1	238	5	58	10	36
	2	342	26	255	40	148
	4	179	26	305	106	471
Fibroblasts γ rays (9)	0	183	1	8	0	0
	0.9	53	2	11	1	4
	1.8	190	17	97	6	19
	3.6	197	10	226	30	100
Fibroblasts α particles	0	137	4	6	0	0
	0.1	62	3	18	7	23
	0.2	81	6	43	11	37
	0.4	57	2	49	18	64
	0.6	43	3	40	15	63
Lymphocytes Fe ions	0	98	9	2	0	0
	0.2	191	8	20	19	78
	0.4	179	13	40	24	87
	0.7	196	29	83	48	194
	1.0	189	33	99	69	338
	1.5	218	59	177	136	722

TABLE 2

Parameters for Total Breakpoint Dose Response Fits

Cell radiation	Model*	α (D)	β (D^2)	c (Intercept)
Gamma lymphocytes	α/β	0.40 ± 0.08	0.29 ± 0.02	0.03 ± 0.06
Gamma fibroblasts	α/β	0.45 ± 0.06	0.09 ± 0.02	0.08 ± 0.04
Alpha particles fibroblasts	Linear	6.76 ± 0.37		0.21 ± 0.08
Fe ions lymphocytes	α/β	1.87 ± 0.18	1.00 ± 0.12	0.17 ± 0.05

*By standard practice, we have fit the γ-ray data to linear-quadratic (α/β) models even though such models failed to provide a significantly better fit to the data than simple linear ones. In the case of Fe ions, an α/β model provided a significantly better fit than a simple linear one (F test, $P < 0.01$).

TABLE 3

Parameters for Chromosome Exchange and Breakpoint Doses Response Fits

Damage parameter	Cell, radiation	Model*	α (D)	β (D^2)	c (Intercept)
Simple exchanges	Fibroblasts γ rays	α/β	0.20 ± 0.05	0.03 ± 0.01	0.03 ± 0.04
	Lymphocytes γ rays	α/β	0.27 ± 0.10	0.04 ± 0.02	–0.004 ± 0.080
	Fibroblasts α particles	Linear	2.02 ± 0.16		0.07 ± 0.04
	Lymphocytes Fe ions	Linear	0.53 ± 0.02		0.02 ± 0.02
Complex exchanges	Fibroblasts γ rays	Quadratic		0.012 ± 0.001	0.002 ± 0.005
	Lymphocytes γ rays	Quadratic		0.037 ± 0.002	–0.007 ± 0.001
	Fibroblasts α particles	Linear	0.75 ± 0.09		0.009 ± 0.021
	Lymphocytes Fe ions	Linear	0.40 ± 0.02		–0.01 ± 0.02
Complex chromosome breakpoints	Fibroblasts γ rays	Quadratic		0.038 ± 0.003	0.01 ± 0.02
	Lymphocytes γ rays	Quadratic		0.17 ± 0.01	–0.07 ± 0.09
	Fibroblasts α particles	Linear	2.70 ± 0.32		0.015 ± 0.074
	Lymphocytes Fe ions	α/β	0.53 ± 0.31	1.16 ± 0.20	0.10 ± 0.09

*By standard practice, we have fit the γ-ray data to linear-quadratic (α/β) models even though such models failed to provide a significantly better fit to the data than simple linear ones. The γ-ray responses for complex exchange breakpoints, however, were fit by pure quadratic models since linear-quadratic fits returned negative α coefficients.